Geophysical Journal International

Geophys. J. Int. (2010) **182,** 797–807 doi: 10.1111/j.1365-246X.2010.04669.x

Propagation of atmospheric model errors to gravity potential harmonics—impact on GRACE de-aliasing

L. Zenner,[1] T. Gruber,[1] A. Jäggi[2] and G. Beutler[2]

[1] *Institute for Astronomical and Physical Geodesy, Technische Universität München, Arcisstr.* 21, 80290 *Munich, Germany. E-mail: zenner@bv.tum.de*
[2] *Astronomical Institute, University of Bern, Sidlerstr.* 5, 3012 *Bern, Switzerland*

Accepted 2010 May 17. Received 2010 April 12; in original form 2009 December 8

SUMMARY

High-frequency, time-varying mass redistributions in the ocean and atmosphere have an impact on GRACE gravity field solutions due to the space–time sampling characteristics of signal and orbit. Consequently, aliasing of these signals into the GRACE observations is present and needs to be taken into account during data analysis by applying atmospheric and oceanic model data (de-aliasing). As the accuracy predicted prior to launch could not yet be achieved in the analysis of real GRACE data, the de-aliasing process and related geophysical model uncertainties are regarded as a potential error source in GRACE gravity field determination. Therefore, this study aims to improve the de-aliasing process in order to obtain a more accurate GRACE gravity field time-series. As these time-series provide estimates for the integrated mass transport in the Earth system, like the global water cycle and solid Earth geophysical processes, any increase in accuracy will lead to improvements in the geophysical interpretation of the results. So in conclusion, improving the de-aliasing is of relevance for a better understanding of geophysical processes. By no longer regarding the atmosphere and ocean model output as error-free, deeper insight into the impact of such uncertainties on the de-aliasing and on the resulting GRACE gravity field models can be obtained. For this purpose, in a first step, a full error propagation of the atmospheric and oceanic model parameters up to the de-aliasing gravity field coefficients is performed and the GRACE K-Band-Satellite-to-Satellite Tracking (KBR-SST) residuals, as an intermediate gravity field result, are analysed. The paper reviews the standard GRACE de-aliasing process and presents the mathematical model applied for the error propagation. Specifically, the effect of uncertainties in the atmospheric input parameters (temperature, surface pressure, specific humidity, geopotential) on the gravity field potential coefficients used for de-aliasing is shown in several scenarios. Finally, the impact of de-aliasing products (with and without error propagation) on a GRACE gravity field solution is investigated on the level of observation residuals. From the results obtained in this study it can be concluded that with respect to the current GRACE error budget, atmospheric model uncertainties do not play a prominent role in the error budget of current GRACE gravity field solutions. Nevertheless, in order to fully exploit the GRACE measurements towards the baseline accuracy, an optimized de-aliasing is needed. In this case, GRACE gravity field solutions are sensitive to uncertainties in atmospheric and oceanic models. Thus, the associated geophysical model errors shall be taken into account in the de-aliasing process.

Key words: Satellite geodesy; Time variable gravity.

1 INTRODUCTION

Mass redistributions inside, on, and above the Earth's surface are responsible for time variable gravity field forces, which directly influence a satellite's orbit. In case these variations have a frequency above the Nyquist frequency, which is defined by the repeat period of a satellite orbit, one has to take into account these mass variations during orbit determination in order to avoid aliasing due to undersampling. In case of a non-repeat cycle orbit (as for GRACE) one has to analyse the sampling characteristics of the actual orbit beforehand in order to identify the frequency, where aliasing will start to have impact on the resulting gravity field solutions. It is obvious that mass variations by tidal forces and in the coupled atmosphere–ocean system occur by far with higher frequencies than the Nyquist frequency of a single satellite mission. As the GRACE observable is a distance (or distance change) between two satellites

(separation approximately 220 km), in this context GRACE also has to be regarded as a single satellite mission, because no multiple observations are taken simultaneously at different locations. What concerns the signal strength, apart from ocean, atmosphere and Earth tides, which are taken into account in the gravity field determination process by models, also non-tidal atmospheric and oceanic mass variations have a strong impact on the GRACE microwave ranging system and cause aliasing, if not taken into account properly (Han *et al.* 2004). Therefore, in the standard GRACE data processing, the high-frequency atmospheric and oceanic signals are modelled and removed during the data analysis. This process is called high-frequency atmospheric and oceanic de-aliasing (AOD) and is described in Flechtner (2007). In addition it should be mentioned here that high-frequency in our context means that a multiyear mean is subtracted and that only deviations from this mean are taken into account and analysed spectrally. As the quality of the GRACE gravity field solutions is still above the simulated prelaunch baseline accuracy, all contributing error sources have to be investigated and analysed in detail. One potential error source could be the de-aliasing process and uncertainties of the geophysical models applied during this process. In this paper, we concentrate on the high-frequency de-aliasing due to atmospheric and oceanic mass variations and investigate in detail, if and how it could be improved. The improvement of GRACE gravity field solution is essential for many applications. Geophysicist, for example, interpret the GRACE measurements in terms of various geophysical processes based on models and observations. It was shown in several studies that GRACE is of sufficient quality to observe effects of co- and post-seismic deformations (e.g. Sumatra earthquake, Chen *et al.* 2007). GRACE is also used to better model and calibrate geophysical fluid processes (Werth *et al.* 2009). On the other hand, geophysical models are input to GRACE data analysis. Improved models will lead to more accurate GRACE measurements and vice versa. GRACE, therefore, links geodetic and geophysical research aspects. Generating more accurate GRACE gravity field solutions will help us to better analyse and understand the mass redistributions on and in the Earth. The paper is structured as follows: First, the de-aliasing process and its fundamental formulas are reviewed, with the main focus on the atmosphere (Section 2.1). As the standard processing scheme assumes error-free atmospheric and oceanic parameters and as it is well known that in areas with sparse observations the atmospheric models are degraded in quality (Salstein *et al.* 2008), there is some motivation to assume, that by taking into account uncertainties of the atmospheric and oceanic model parameters one could improve the de-aliasing product and consequently the gravity field solutions. This is why a mathematical model of error propagation of the atmospheric model uncertainties into the gravity field de-aliasing coefficients was developed. The processing strategy and the formulas to be applied are shown in Sections 2.2 and 2.3. In order to investigate the impact of atmospheric model uncertainties on intermediate gravity field results, a test environment based on a real GRACE data set, data from the European Center for Medium Range Weather Forecast (ECMWF) operational atmospheric analysis (ECMWF 2009), and from the Ocean Model for Circulation and Tides (OMCT) (Dobslaw & Thomas 2007) was set up. Detailed information about the OMCT and its use for AOD can be found in Flechtner (2007). In our preliminary analysis, in a first step, the dominating error parameters of the atmospheric model are identified. For this purpose, uncertainties of the atmospheric parameters and their propagation are treated individually. Results are shown in Section 3.1. In our investigations the ocean model is assumed as error-free. Only the impact of atmospheric uncertainties is described exemplarily. In Section 3.2, the impact of the atmospheric error assumptions on the estimated de-aliasing coefficients and on the derived geoid is investigated. Differences between the error-free and error scenario are computed and compared to the GRACE error predictions. Finally, the newly computed de-aliasing coefficients are applied within a GRACE gravity field determination. In order to identify their impact on the resulting gravity field solution, KBR-SST residuals are investigated in detail (Section 3.3). Section 4 summarizes the results and provides some conclusions of this work.

2 THEORY: THE DE-ALIASING PROCESS

2.1 The standard de-aliasing process

This section provides a short overview of the fundamental formulas of the nominal atmospheric and oceanic de-aliasing processing sequence. It should be mentioned that in principle there are two methods of taking the atmospheric mass variations into account: the first one is the so-called 'surface pressure' approach, the second one the 'vertical integration' (VI) approach. As investigations have shown that for high precision applications the vertical structure of the atmosphere has to be taken into account, the latter is used in the standard GRACE data processing in order to reach ultimate accuracy (Flechtner 2007).

Input parameters needed for the determination of the atmospheric potential are for the atmosphere: point values of surface pressure P_s and geopotential height H_s grids (e.g. $1^\circ \times 1^\circ$) on the Earth's surface as well as point values of temperature T and specific humidity S at all 91 levels of the atmospheric model at different time steps (e.g. 6 hr). The data used for de-aliasing is taken from operational analysis ECMWF (ECMWF 2009). Ocean bottom pressure grids P_{O} are taken from OMCT (Dobslaw & Thomas 2007), which is forced by ECMWF operational analysis data, too. The most important equations for the VI approach are summarized in the following (details are given in Flechtner 2007)

$$P_{k+1/2} = a_{k+1/2} + b_{k+1/2} P_s \tag{1}$$

$$T_v = (1 + 0.608S)T \tag{2}$$

$$H_{k+1/2} = H_s + \sum_{j=k+1}^{k_{\max}} \frac{RT_v}{g} \ln\left(\frac{P_{j+1/2}}{P_{j-1/2}}\right) \tag{3}$$

$$\left.\begin{matrix}\bar{C}_{nm} \\ \bar{S}_{nm}\end{matrix}\right\} = \frac{-a^2(1+k'_n)}{(2n+1)Mg} \int_\theta \int_\lambda [I_n + P_{\mathrm{O}}] \bar{P}_{nm}(\cos\theta) \left\{\begin{matrix}\cos m\lambda \\ \sin m\lambda\end{matrix}\right\} \sin\theta \,\mathrm{d}\theta \,\mathrm{d}\lambda \tag{4}$$

$$I_n = \int_{P_s}^{0} \left(\frac{a}{a - H_{k+1/2}} + \frac{N'}{a}\right)^{n+4} \mathrm{d}P, \tag{5}$$

where $P_{k+1/2}$ is the pressure at half-levels, $a_{k+1/2}$, $b_{k+1/2}$ is the model dependent coefficients, P_s is the surface pressure, S is the full-level specific humidity defined at multilevels k ($k = 0{:}91$), T is the full-level temperature defined at multilevels k, T_v is the full-level virtual temperature defined at multilevels k, R is the gas constant for dry air, $H_{k+1/2}$ is the geopotential height at half-levels, H_s is the surface geopotential height (full-level), g is the mean

gravity acceleration, a is the semi-major axis of reference ellipsoid, M is the Earth mass, k'_n is the loading love numbers, P_{O} is the ocean bottom pressure, I_n is the vertically integrated atmospheric pressure, I_n^{ref} is the mean vertically integrated atmospheric pressure, $P_{\mathrm{O}}^{\mathrm{ref}}$ is the mean ocean bottom pressure, $\bar{P}_{nm}$ is the associated normalized legendre polynomials and N' is the mean geoid height above the sphere $r = a$.

In a first step, the pressure $P_{k+1/2}$ at all model half-levels $k + 1/2$ and the virtual temperature at all model full-levels k are computed according to eqs (1) and (2). Pressure, virtual temperature, and the surface geopotential heights H_s are then used to calculate the geopotential heights $H_{k+1/2}$ for all levels according to eq. (3). Afterwards, eq. (5) is used to perform the vertical integration numerically for each degree separately. Before the atmosphere is combined with the ocean, a mean vertically integrated field I_n^{ref} and a mean ocean field $P_{\mathrm{O}}^{\mathrm{ref}}$ are usually subtracted beforehand from the instantaneous atmospheric pressure I_n as well as from the ocean bottom pressure P_{O} in order to analyse gravitational variations. As the mean mass distribution of the atmosphere and ocean by definition refers to the static part of the gravity field, only the deviations from the mean value have to be taken into account for the de-aliasing process in order to remove the short-term gravitational variations. In the currently realized GRACE gravity field processing as well as in our investigations, mean fields obtained from the years 2001+2002 are used. For more details we refer again to Flechtner (2007). The combined residual atmospheric and oceanic pressure

$$P_{\mathrm{AO}} = \Delta I_n + \Delta P_{\mathrm{O}} = I_n - I_n^{\mathrm{ref}} + P_{\mathrm{O}} - P_{\mathrm{O}}^{\mathrm{ref}} \tag{6}$$

is stored in a 3-D array with longitude, latitude and degree as indices. Finally, the numerical integration is performed within eq. (4). The 3-D matrix, stored as an intermediate result, serves as input for the spherical harmonic analysis (SHA) by numerical integration. The SHA is also performed separately for each degree of the spherical harmonic series in order to take into account the degree-dependent exponent in eq. (5). The result of the numerical integration are the combined atmospheric and oceanic potential coefficients $\bar{C}_{nm}, \bar{S}_{nm}$ (official AOD1B product, Flechtner 2007).

2.2 Mathematical method of error propagation for the atmospheric and oceanic de-aliasing process

As outlined in Section 1, the VI input parameters temperature T, specific humidity S, surface pressure P_s, surface geopotential height H_s and ocean bottom pressure P_{O} have so far been assumed to be error-free, although it is well-known that there are large uncertainties, in particular in the atmospheric surface pressure (Ponte & Dorandeau 2003). One of the goals of this work is to quantify the effect of uncertainties in T, S, P_s, H_s and ocean bottom pressure P_{O} on the resulting de-aliasing coefficients $\bar{C}_{nm}, \bar{S}_{nm}$. Therefore, in a first step, we applied a mathematical model to propagate the atmospheric field errors ($\sigma_T, \sigma_S, \sigma_{P_s}, \sigma_{H_s}$) into the pressure errors (σ_{I_n}) at the centre of mass of the atmospheric column I_n. The principle and the applied formulas are summarized below.

Neglecting the covariances between the atmospheric and oceanic input parameters, the simplified law of error propagation can be applied

$$f(x, y) \Rightarrow \sigma_f = \left[\left(\frac{\partial f}{\partial x} \right)^2 \sigma_x^2 + \left(\frac{\partial f}{\partial y} \right)^2 \sigma_y^2 \right]^{\frac{1}{2}}. \tag{7}$$

Eq. (7) states that the error σ_f of a function f depending on x and y can be determined from the uncertainties σ_x and σ_y of x and y and the partial derivatives of f with respect to x and y. Applying this simplified law of error propagation step by step to the above-mentioned sequence of formulas (eqs 1–3 and 5) we get

(i) For the error of virtual temperature

$$\begin{aligned} T_v &= (1 + 0.608S)T \\ \Rightarrow \quad \sigma_{T_v} &= \left[\left(\frac{\partial T_v}{\partial T} \right)^2 \sigma_T^2 + \left(\frac{\partial T_v}{\partial S} \right)^2 \sigma_S^2 \right]^{\frac{1}{2}} \end{aligned} \tag{8}$$

with the partial derivatives

$$\begin{aligned} \frac{\partial T_v}{\partial T} &= 1 + 0.608S \\ \frac{\partial T_v}{\partial S} &= 0.608T \end{aligned}$$

(ii) For the error of the 'half-level' pressure

$$\begin{aligned} P_{k+1/2} &= a_{k+1/2} + b_{k+1/2}\, P_s \\ \Rightarrow \sigma_{P_{k+1/2}} &= \left[\left(\frac{\partial P_{k+1/2}}{\partial P_s} \right)^2 \sigma_{P_s}^2 \right]^{\frac{1}{2}} \end{aligned} \tag{9}$$

with the partial derivative

$$\frac{\partial P_{k+1/2}}{\partial P_s} = \quad b_{k+1/2.}$$

(iii) For the error of the geopotential height in 'half-levels'

$$\begin{aligned} H_{k+1/2} &= H_s + \sum_{j=k+1}^{k_{\max}} \frac{R T_v}{g} \ln \left(\frac{P_{j+1/2}}{P_{j-1/2}} \right) \\ \Rightarrow \sigma_{H_{k+1/2}} &= \left[\left(\frac{\partial H_{k+1/2}}{\partial T_v} \right)^2 \sigma_{T_v}^2 + \ldots \right. \\ &\quad + \left(\frac{\partial H_{k+1/2}}{\partial P_{j+1/2}} \right)^2 \sigma_{P_{j+1/2}}^2 + \ldots \\ &\quad \left. + \left(\frac{\partial H_{k+1/2}}{\partial P_{j-1/2}} \right)^2 \sigma_{P_{j-1/2}}^2 + \sigma_{H_s}^2 \right]^{\frac{1}{2}} \end{aligned} \tag{10}$$

with the partial derivatives

$$\begin{aligned} \frac{\partial H_{k+1/2}}{\partial T_v} &= \frac{1}{g} \sum_{j=k+1}^{k_{\max}} R \ln \left(\frac{P_{j+1/2}}{P_{j-1/2}} \right) \\ \frac{\partial H_{k+1/2}}{\partial P_{j+1/2}} &= \frac{1}{g} \sum_{j=k+1}^{k_{\max}} R T_v \left(\frac{1}{P_{j+1/2}} \right) \\ \frac{\partial H_{k+1/2}}{\partial P_{j-1/2}} &= -\frac{1}{g} \sum_{j=k+1}^{k_{\max}} R T_v \left(\frac{1}{P_{j-1/2}} \right). \end{aligned}$$

(iv) For the error of the pressure at the centre of mass of the atmospheric column

$$\begin{aligned} I_n &= \int_{P_s}^{0} \left(\frac{a}{a - H_{k+1/2}} + \frac{N'}{a} \right)^{n+4} \mathrm{d}P \quad \Rightarrow \\ \sigma_{I_n} &= \left[\left(\frac{\partial I_n}{\partial H_{k+1/2}} \right)^2 \sigma_{H_{k+1/2}}^2 + \left(\frac{\partial I_n}{\partial \mathrm{d}P} \right)^2 \sigma_{\mathrm{d}P}^2 \right]^{\frac{1}{2}} \end{aligned} \tag{11}$$

with the partial derivatives

$$\frac{\partial I_n}{\partial H_{k+1/2}} = \int_{P_s}^{0} (n+4)\left(\frac{a}{a-H_{k+1/2}} + \frac{N'}{a}\right)^{n+3} \left[-\frac{a}{\left(a-H_{k+1/2}\right)^2}\right] \mathrm{d}P$$

$$\frac{\partial I_n}{\partial \mathrm{d}P} = \left(\frac{a}{a-H_{k+1/2}} + \frac{N'}{a}\right)^{n+4}$$

with $\mathrm{d}P = P_{k+1/2} - P_{k-1/2} \Rightarrow \sigma_{\mathrm{d}P} = (\sigma^2_{P_{k+1/2}} + \sigma^2_{P_{k-1/2}})^{\frac{1}{2}}$.

(v) and finally for the error of the combined atmospheric and oceanic pressure

$$P_{\mathrm{AO}} = \Delta I_n + \Delta P_{\mathrm{O}} \Rightarrow \sigma_{P_{\mathrm{AO}}} = \left(\sigma^2_{\Delta I_n} + \sigma^2_{\Delta P_{\mathrm{O}}}\right)^{\frac{1}{2}}. \quad (12)$$

Eqs (8)–(12) provide an opportunity to propagate uncertainties in the atmospheric input parameters into the vertically integrated atmospheric pressure I_n as well as on the combined atmospheric and oceanic pressure P_{AO}. The effect of errors in the various input parameters on the atmospheric pressure is discussed and illustrated in Section 3.1.

2.3 Determination of de-aliasing potential coefficients by least squares adjustment

In order to reach our goal of determining the effect of model uncertainties on the AOD product, the error of the combined atmospheric and oceanic pressure $\sigma_{P_{\mathrm{AO}}}$ has to be further propagated into the potential coefficients. To do this, the present de-aliasing processing sequence is modified as it is shown in Fig. 1. As mentioned in Section 2.1, in the standard GRACE de-aliasing process the spherical harmonic analysis is performed by a numerical integration of P_{AO} for each degree separately (*cf.* eq. 4). Uncertainties in P_{AO} are not yet considered. In order to take the uncertainties in the combined residual atmospheric and oceanic pressure into account and to determine the effect of input parameter errors on the de-aliasing coefficients $\bar{C}_{nm}$, $\bar{S}_{nm}$, the present approach of numerical integration is replaced by a least-squares adjustment (Gauss–Markov model). For this, eq. (4) is substituted by the observation eq. (13). (For further details on the principle and modelling of gravity field determination we refer to Gruber 2001).

$$P_{\mathrm{AO}} = -\frac{Mg}{a^2}\sum_n \frac{2n+1}{1+k'_n}\sum_m \bar{P}_{nm}(\cos\theta) \left[\bar{C}_{nm}\cos m\lambda + \bar{S}_{nm}\sin m\lambda\right], \quad (13)$$

and the basic formulas for least-squares adjustment

$$Ax = l + v \qquad \hat{x} = (A^T PA)^{-1} A^T Pl \quad (14)$$

are applied, where $\hat{x}$ are the adjusted unknowns x, l the observations, and P the weighting matrix. In our context the unknowns x are the atmospheric and oceanic potential coefficients $\bar{C}_{nm}$, $\bar{S}_{nm}$. The observations l are the combined residual atmospheric and oceanic pressure values P_{AO} on a global (φ,λ)-grid. To set up the the coefficient-matrix A, the partial derivatives of the observations l with respect to the unknown coefficients $\bar{C}_{nm}$ and $\bar{S}_{nm}$ are determined. Furthermore, the weighting-matrix of the observations P is set up, where P is defined by the uncertainties $\sigma_{P_{\mathrm{AO}}}$ of P_{AO}, which are determined by the error-propagation model shown in Section 2.2. To get the 'new' AOD product, basically three steps are performed (*cf.* Fig. 1). In a first step, the vertically integrated residual atmospheric pressure I_n and its error σ_{I_n} are calculated (via eqs 8–12). Then the atmospheric pressure I_n and the ocean bottom pressure P_{O} as well as the corresponding errors are combined according to eq. (12). In a second step, the normal equation system (NEQ, $A^T PA$) can be set up for each degree separately via the observations P_{AO} and the uncertainties of P_{AO} as individual weights (*cf.* second row in

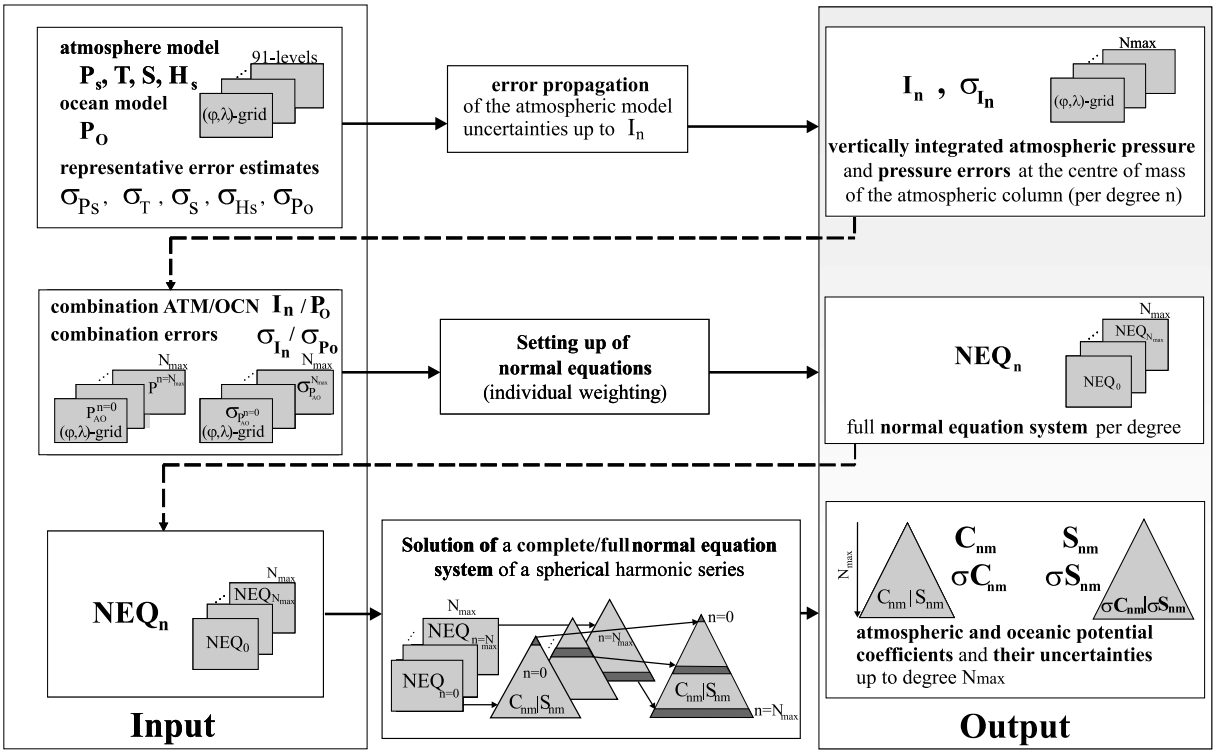

Figure 1. Overview of the de-aliasing processing approach with error propagation.

Fig. 1). Afterwards, every NEQ for each degree of the spherical harmonic series is solved separately. Finally, the complete spherical harmonic series $\bar{C}_{nm}$, $\bar{S}_{nm}$ including its error estimates $\sigma\bar{C}_{nm}$, $\sigma\bar{S}_{nm}$ are obtained (third row in Fig. 1).

3 RESULTS: IMPACT OF ATMOSPHERIC UNCERTAINTIES

Before the effect of model uncertainties on AOD and GRACE is investigated, it has to be made clear that in the following, particularly in Sections 3.2 and 3.3, the oceanic contribution is assumed as error-free, as the determination of reliable ocean bottom pressure values is not trivial. This means that the error of the combined atmospheric and oceanic pressure $\sigma_{P_{\mathrm{AO}}}$ is equal to the error of I_n (*cf.* eq. 12). For the time being only atmospheric uncertainties provided by ECMWF were used to get a first insight into the effect of model errors on AOD and GRACE results.

3.1 Impact of atmospheric model uncertainties on the vertically integrated atmospheric pressure I_n

Using eqs (8)–(11), it is possible to determine the error of the pressure σ_{I_n} at the centre of mass of the atmospheric column due to uncertainties in the input parameters T, S, P_s and H_s. Eq. (13) solved in a least-squares adjustment with individual weighting of P_{AO} (by $1/\sigma^2_{P_{\mathrm{AO}}}$) provides the effect of model uncertainties on the AOD product. Before the effect of model uncertainties on AOD is investigated, the dominating error parameters of the atmospheric model are identified. For this purpose, uncertainties of the atmospheric parameters and their propagation are treated individually. As the determination of representative error measures is still in progress, see for example, Schmidt *et al.* (2008), errors in the analysis, provided by ECMWF are used in our investigations. As for example, the surface pressure error-field, is illustrated in Fig. 2 for one individual point in time. The error-characteristics are not discussed here. Fig. 2 shall merely give a picture of the used error-structure. Fig. 3 gives insight into the impact of each atmospheric input parameter or to be more precise, the impact of uncertainties in each input parameter (Figs 3b–f) on the vertically integrated atmospheric pressure I_n (Fig. 3a). The results are shown for degree $n = 10$. [*Note:* The general pattern and the conclusions which are drawn in the following are valid for each degree $n >= 2$. Basically, only the values in Fig. 3 are slightly increasing or decreasing for higher or lower degrees n because of the degree dependency of I_n and σ_{I_n} (*cf.* eq. 11).] It can be recognized that uncertainties in the specific humidity (Fig. 3e), temperature (Fig. 3c) and geopotential height (Fig. 3d) have only very small effects on the vertical integral I_n with maxima of 0.008, 0.05 and 0.3 Pa, respectively. Uncertainties in the surface pressure (Fig. 3b), on the other hand, have by far the largest effect of up to 750 Pa on the vertical integral I_n. Comparison of Fig. 3(b) with Fig. 3(f) shows that the effect of uncertainties in only the surface pressure and the effect of uncertainties in all four input parameters is virtually the same. This in turn implies that the error of the vertically integrated atmospheric pressure I_n is dominated by the uncertainty of the surface pressure P_s and the errors in temperature, specific humidity, and geopotential height are almost negligible. Therefore, we will only distinguish between the 'full-error' and the 'error-free' scenario in the following (*cf.* Section 3.2).

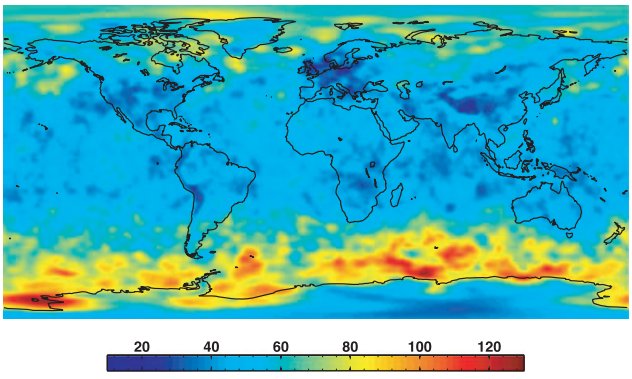

Figure 2. Error of ECMWF, operational analysis surface pressure on 01.08.2007 00h. Unit: Pascal.

It has been shown within our investigations that whether the uncertainties are taken into account or not affects the pressure at the centre of mass of the atmospheric column in the range of 143–754 Pa or, equivalently, 15–77 mm water column, which on average is about 0.7 per cent of the total vertically integrated atmospheric pressure or about 7 per cent of the residual vertically integrated atmospheric pressure. The question that now arises is: do the uncertainties in the atmospheric pressure of up to 7.5 hPa significantly affect AOD and GRACE results or not?

3.2 Impact of atmospheric uncertainties on de-aliasing coefficients and the geoid

In order to answer this question we performed two error-scenarios

(1) 'error-free' AOD: The uncertainties of the atmospheric parameters are not taken into account corresponding to equal weighting of the input parameters, and
(2) 'full-error' AOD: The uncertainties of the atmospheric parameters are taken into account.

The 'error-free' experiment thus assumes that all observations P_{AO} have the same weights and the 'full-error' scenario assumes that the observations P_{AO} are weighted individually using $1/\sigma^2_{P_{\mathrm{AO}}}$ on the diagonal of the P matrix. In this study the ocean bottom pressure is error-free, and $\sigma^2_{P_{\mathrm{AO}}}$ becomes $\sigma^2_{I_n}$. After performing the least-squares adjustment for these two scenarios, two sets of AOD products are obtained. Their difference provides insight into the effect of taking atmospheric uncertainties into account or not. (In order to keep the computational effort (adequately) small, the maximum degree n was limited to 30 in our current investigations).

Fig. 4 shows the differences between 'full-error' and the 'error-free' AOD coefficients. It can be seen that the maximum effect on the potential coefficients (Fig. 4a) is up to 10^{-11}. This seems to be quite small, but compared to the magnitude of the AOD coefficients itself, it seems that the differences are not negligible. The latter statement is confirmed if we inspect the differences of the two error scenarios in terms of degree variances (Fig. 4b). The difference between the two error-scenarios is presented in the red line. Compared to the GRACE baseline (lowest line in Fig. 4b) the effect of atmospheric model uncertainties clearly is in the sensitivity range of GRACE. Fig. 5 shows the effect of atmospheric model uncertainties on the geoid with a range of −0.8 to 0.3 mm. Comparing Figs 3(f) and 5, some 'inverse correlation-patterns' can be recognized. The reason for this is the deviation between the two error-scenarios, namely the different weighting of the observations P_{AO}. Therefore, the error of the atmospheric pressure is reflected in the difference between the two error-scenarios. Larger discrepancies should appear in regions where the weights for the observations are extreme (high or low).

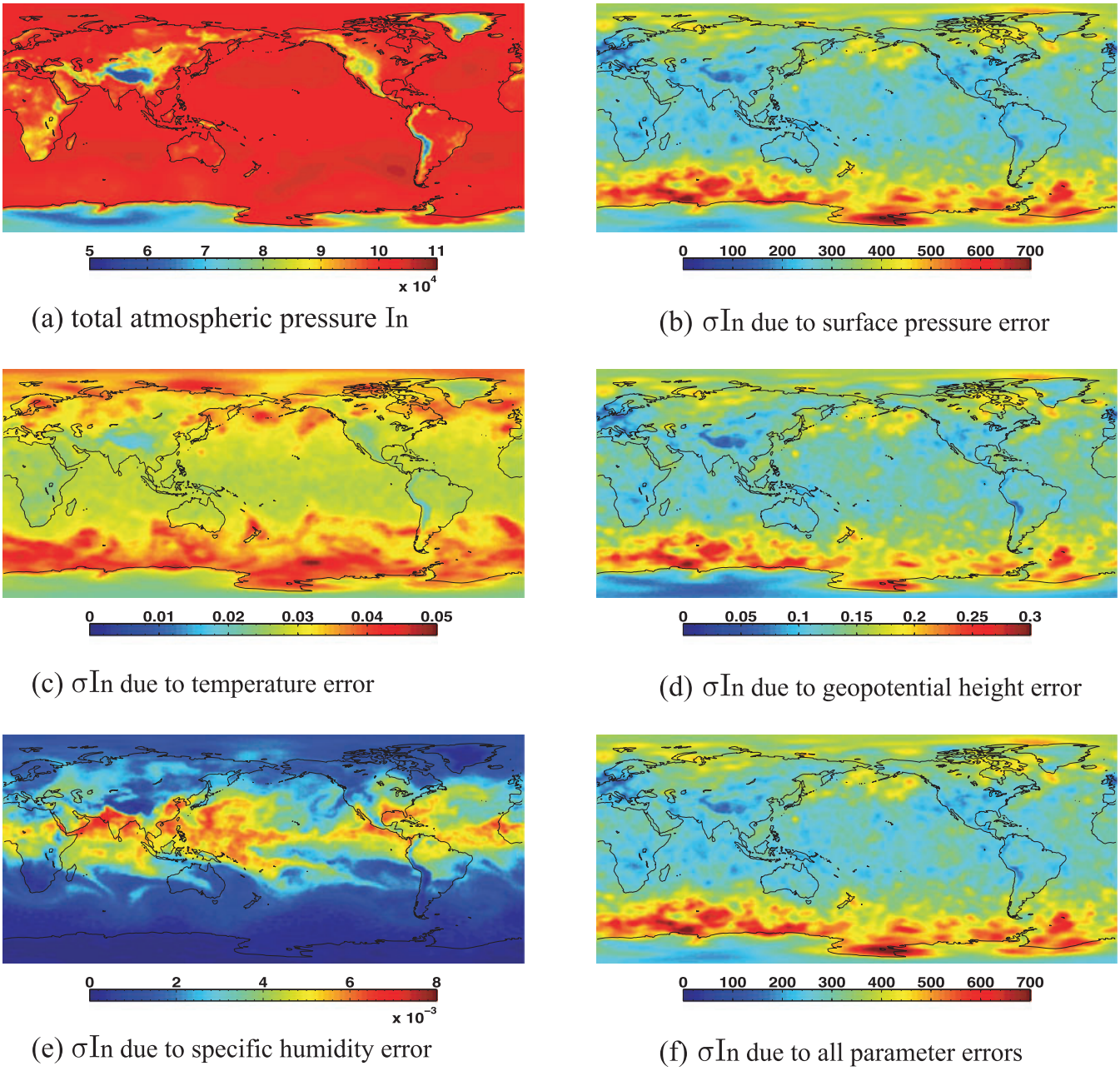

Figure 3. Vertically integrated atmospheric pressure I_n (a) and the error σ_{I_n} of the vertical integral due to uncertainties in the four input parameters (b–f), Unit: Pascal, $n = 10$, 01.08.2007 00h.

This is exactly what can be seen in Fig. 5, for example, in the Himalaya region. The error of the vertically integrated atmospheric pressure in this region is quite small compared to other regions (Fig. 3f). This in turn means that compared to the 'error-free' case, this region will be weighted 'higher' in the 'full-error' case, which finally leads to higher differences in these regions between the two scenarios.

Let us resume the discussion of whether atmospheric model uncertainties have a significant effect on AOD and GRACE or not. This Section has shown that atmospheric model uncertainties affect the VI component of the AOD product in terms of geoid heights in the sub-mm domain. Compared to the GRACE baseline (blue in Fig. 4b), the effect of atmospheric model uncertainties clearly is in the sensitivity range of GRACE. Therefore, we conclude that an effect should be visible in the gravity field solution as well. This aspect will be studied in Section 3.3.

3.3 Impact on GRACE K-band residuals

In the course of gravity field modelling, which can be seen as an extended orbit determination problem, one tries to minimize the differences between the computed observations based on *a priori* models and the real observations made by GRACE by only adjusting orbit parameters. The computed observations would represent the real observations, if all force models (tides, static gravity field, AOD-model, etc.) as well as the real observations were error-free. As this is not the case, differences to the real observations occur. For

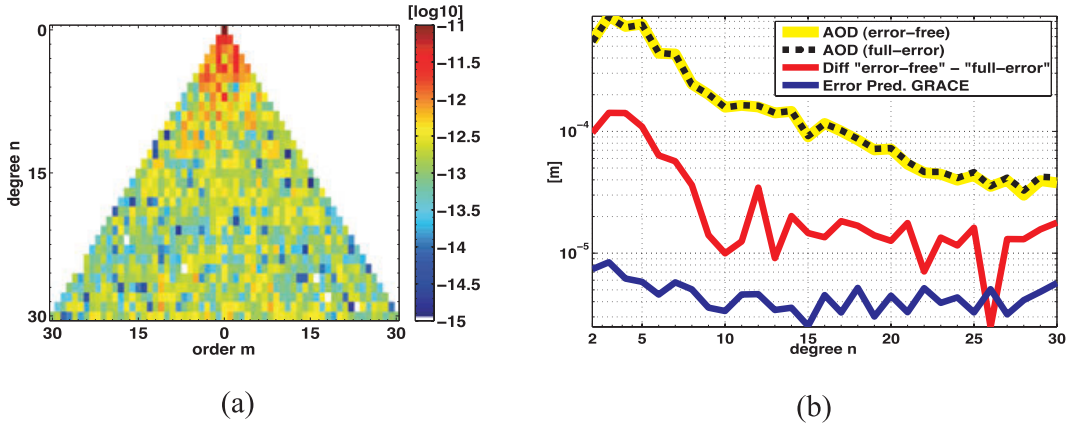

Figure 4. Differences between the 'error-free' AOD and 'full-error' AOD in terms of (a) potential coefficients (Unit: dimensionless, log10) and in terms of (b) degree variances for geoid heights (Unit: m), 01.08.2007 00h

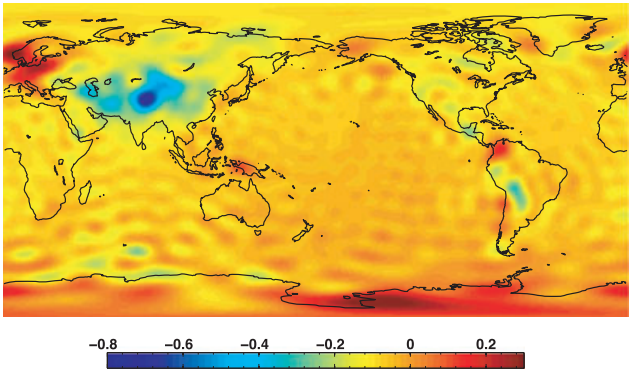

Figure 5. Difference between the 'error-free' and 'full-error' scenario in terms of geoid heights. Unit: mm, 01.08.2007 00h.

GRACE, basically intersatellite range-rates are computed and compared to the measured ones. K-band range-rate (KBRR) residuals as an intermediate result during gravity field modelling are analysed. The KBRR-residuals contain all model errors, measurement errors, and unmodelled forces. By applying the new de-aliasing coefficients, which take the atmospheric model uncertainties into account, we hope to reduce these residuals. This would imply that the new ('full-error') AOD product is more realistic than the standard or 'error-free' AOD.

For this purpose the Bernese GPS Software (Dach *et al.* 2007) and the Celestial Mechanics Approach (Beutler *et al.* 2010) is used to perform an orbit determination based on kinematic positions and KBRR observations by using the gravity field model AIUB-GRACE02S (for further details on, for example, underlying background models, we refer to Jäggi *et al.* 2010). During gravity field modelling only the AOD coefficients are changed. By leaving all other settings unchanged, we get insight into the effect of using alternative AOD products. In addition to the two error-scenarios described in Section 3.2, the overall effect of AOD by simply applying no AOD product during gravity field modelling is included as well. The impact of the three experiments on KBRR-residuals is shown in Fig. 6. Applying (blue line in Fig. 6a) or not applying (green line in Fig. 6a) AOD clearly reduces the daily KBRR-residuals. Removing the high-frequency atmospheric and oceanic mass variations significantly reduces the daily rms of KBRR-residuals over 1 yr by about 10 per cent (Fig. 6a). A more detailed view of the residuals in Fig. 6(b) shows that the amplitudes of the dominant peaks are reduced, but not completely removed, when applying AOD. One reason for this might be the fact that AIUB-GRACE02S is a static field where the time-variable signals mainly from unmodelled seasonal hydrology are not yet modelled. However, in general, the signal in the residual series is reduced.

The interesting question is, if the 'full-error' AOD could be able to further improve de-aliasing, that is, to further reduce

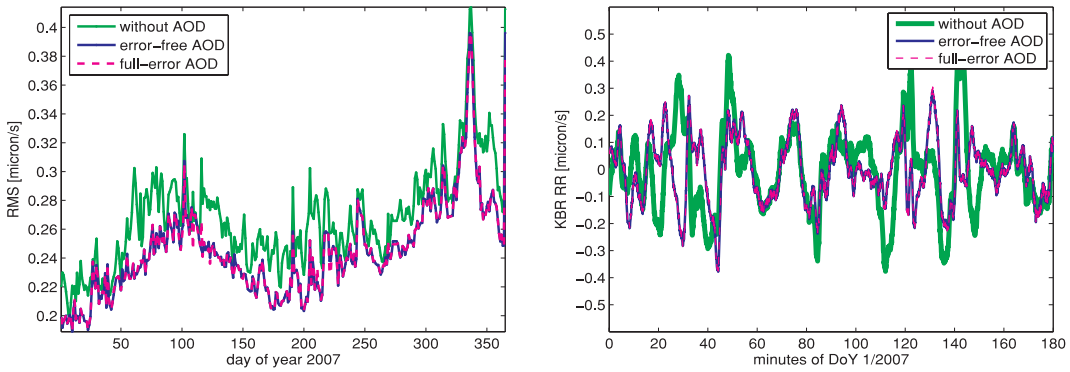

Figure 6. (a) Daily rms of KBRR-residuals for 2007 without AOD (green), after removing the 'error-free' AOD (blue) and 'full-error' AOD (dotted magenta line); (b) KBRR-residuals for first 3 hr of DoY 1/2007 (notice different colouring). Unit: in $\mu m\,s^{-1}$.

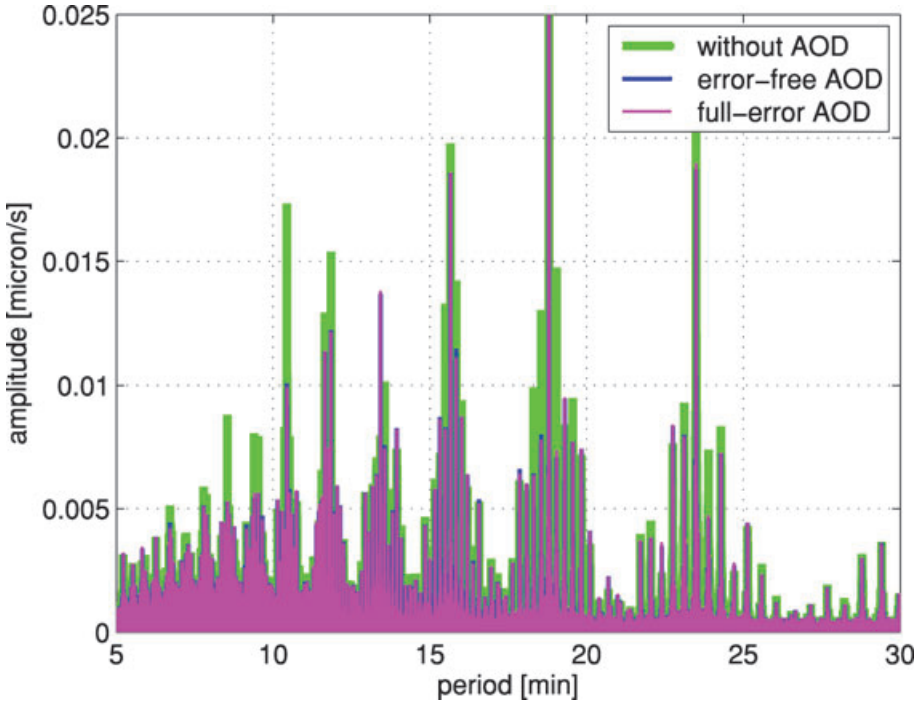

Figure 7. Spectra of 1 yr (2007) KBRR-residuals without AOD (green), after removing 'error-free' AOD (blue) and 'full-error' AOD (magenta line). Unit: μm s^{-1}

KBRR-residuals? Fig. 6 (magenta dashed line) illustrates that this is not the case, as the remaining residuals cannot be further reduced significantly by applying atmospheric error characteristics. The three experiments can also be analysed in the frequency domain by computing amplitude spectra. The results are shown in Fig. 7, where only the amplitudes of the spectral terms with periods in the interval 5 min to 30 min are shown. As in the time-domain, one could also state here that in general the amplitudes of the spectral lines are reduced when applying AOD or not (*cf.* blue and green spectral lines in Fig. 7), but applying the full-error AOD in the standard GRACE data processing has no further significant effect on the amplitude spectra (*cf.* blue and magenta lines in Fig. 7). Another interesting way to represent the KBRR-residuals is to illustrate them geographically as a function of latitude and longitude in an Earth-fixed system. Fig. 8 illustrates the rms values over 1 yr of all residuals in latitude/longitude bins of $5^\circ \times 5^\circ$. Fig. 8(a) shows the rms of KBRR-residuals without applying AOD, while Fig. 8(b) shows the rms after removing the error-free AOD. Both Figures show relatively high rms values in the Amazone, Zambezi, Ganges and Northern polar area, which is caused by the unmodelled temporal variations of the gravity field and which can mainly be addressed to hydrology. The pattern has been expected to be visible in the KBRR-residuals as all other sources of gravity field variation have been modelled in the GRACE data processing. The rms values for the full-error experiment do not differ significantly from the error-free AOD (not shown here). Instead the rms of the differences 'without AOD minus error-free AOD' and 'error-free AOD minus full-error AOD' are shown, in order to get insight into the overall effect of AOD and the new 'full-error' AOD product, which takes model uncertainties into account. Fig. 8(c) shows the total effect of AOD on level of the KBRR-residual differences. Fig. 8(d) illustrates the effect of atmospheric model uncertainties. It again becomes obvious that the effect of taking atmospheric model uncertainties into account compared to the error-free case is pretty small ($\sim$factor 10). Another maybe interesting aspect concerning the geographically representation of residuals is the following: the patterns in both Figs 8(c) and (d) should somehow reflect the models applied during gravity field determination if nothing else than the AOD product is changed during gravity field determination. As mentioned, Fig. 8(c) illustrates the overall effect of (error-free) AOD on the KBRR-residuals. Thus Fig. 8(c) shall reflect the (error free) AOD model being removed during gravity field determination. To confirm this conclusion one should have a look at the rms over 1 yr of the (error-free) AOD coefficients (see Fig. 9a). Comparing the rms of the AOD product in Fig. 9(a) with the effect of AOD on level of KBRR-residuals in Fig. 8(c), we can see some correlations. We find high similarities in the Northern hemisphere (e.g. Europe, North America, Greenland and Northern Asia) but also some similarities in the Southern hemisphere (e.g. West of South America, Western Antarctica and South of Africa). Fig. 8(d) shows the effect of full-error AOD with respect to error-free AOD on level of the residuals. Fig. 8(d) shall therefore reflect the model difference between the error-free and full-error AOD. As it was described in Section 3.2, the only difference between the error-free and full-error scenario is the different weighting of the observations P_{AO}. The weighting equates to the inverse error of P_{AO} which in turn equates in our case to the error of the atmosphere as the ocean bottom pressure is assumed as error-free (*cf.* Section 3.1, eq. 12). Consequently, it can be expected that the error of the atmospheric pressure $\sigma\ I_n$ also maps onto the residuals. Checking the rms of $\sigma\ I_n$ (Fig. 9b) against the effect of atmospheric model uncertainties on residual-level (Fig. 8d), we can also find here correlation patterns (of inverse sign), for example, in the Andes, in the Himalaya region, Europe or Antarctic boundary region. Note that the numerical values between Figs 8(c) and 9(a), as well as between Fig. 8(d) and Fig. 9(b) are not comparable as there is a whole parametrization process

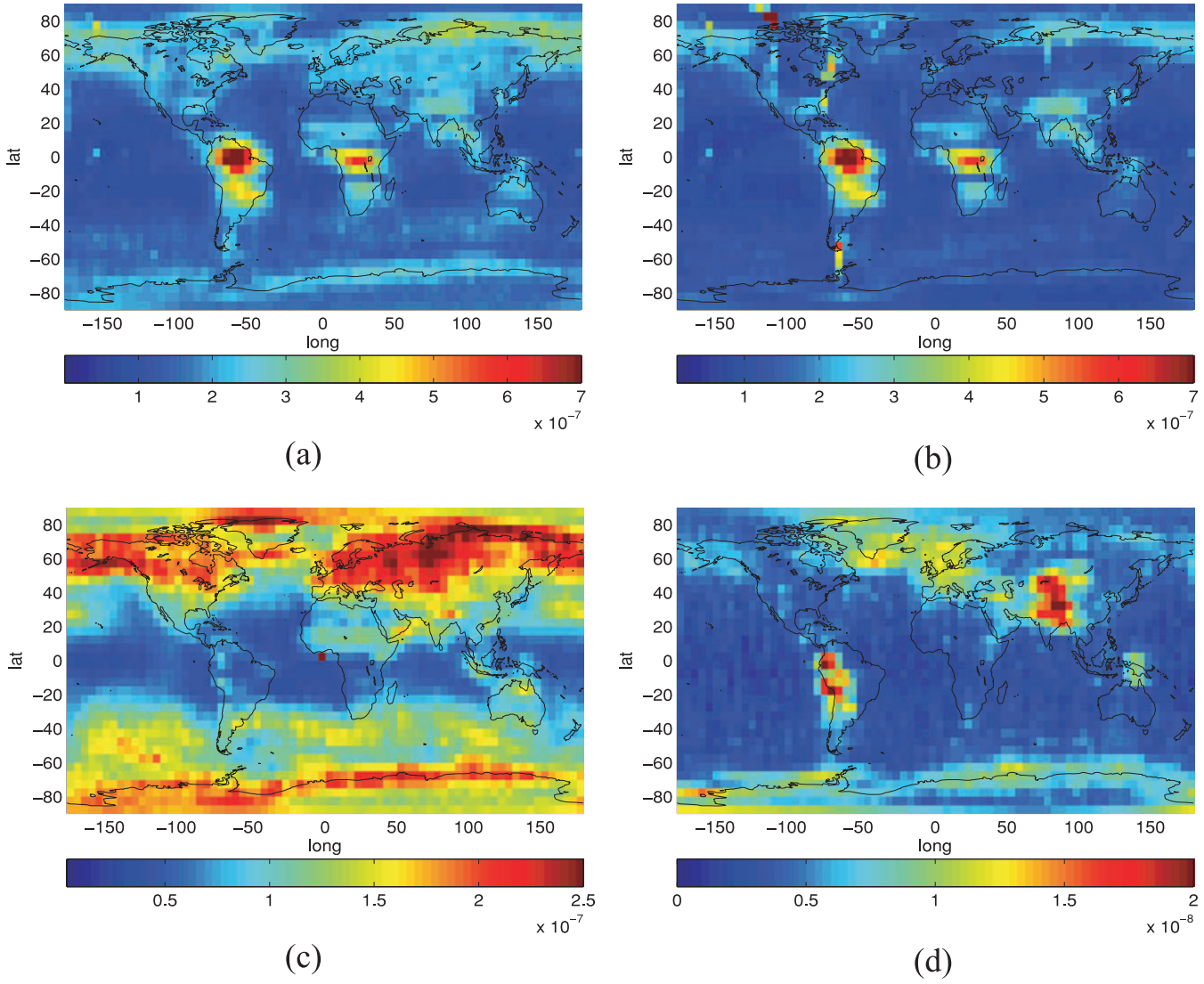

Figure 8. Rms over 1 yr (2007) of KBRR-residuals in bins of 5° × 5° in longitude and latitude. (a) without AOD; (b) error-free AOD; (c) rms of KBRR-residual differences (a) and (b); (d) rms of KBRR-residual differences (b) full-error AOD (rms of KBRR-residuals for full-error AOD experiment not shown here). Unit: m s^{-1}.

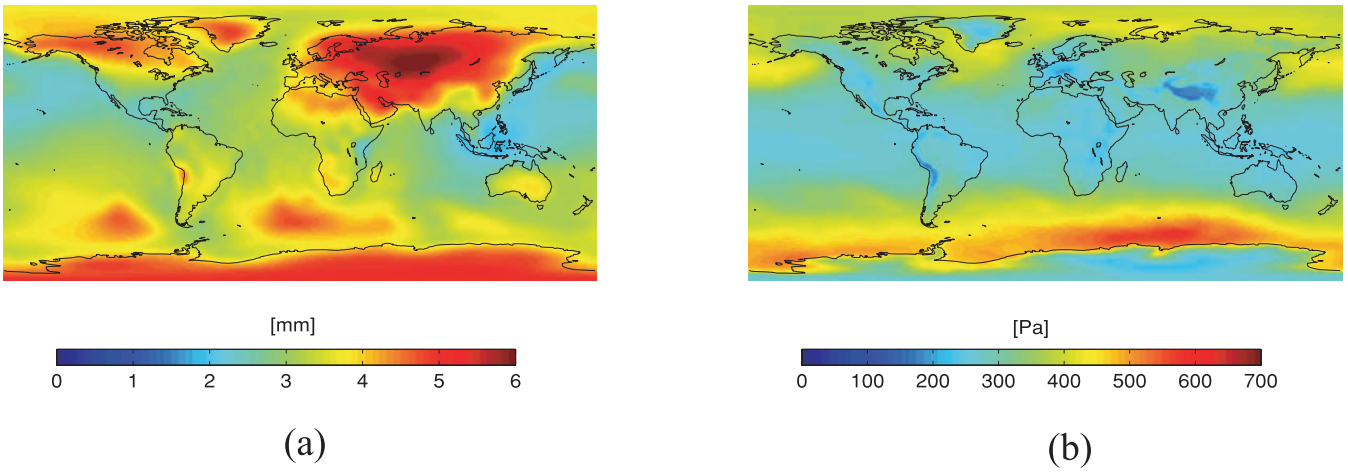

Figure 9. Rms of (a) error-free AOD product over 1 yr in terms of geoid heights (2007, Unit: mm) and (b) rms of error of the vertically integrated atmospheric pressure $\sigma\ I_n$ over 1 yr (2007, Unit: Pascal) Remark: the range of 0–6 mm geoid height equates approximately to a range of 0–140 mm equivalent water height.

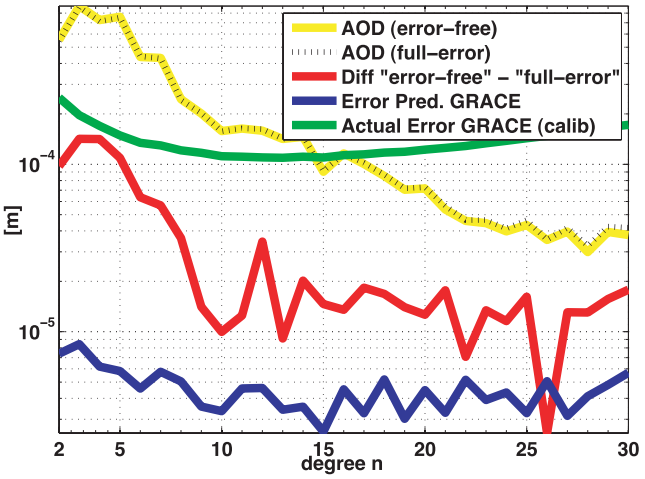

Figure 10. Degree variance differences of error-free AOD and full-error AOD in terms of geoid heights, and the predicted and current GRACE error estimates. Unit: m, 01.08.2007 00h.

in between and thus are not of interest. Figs 9(a) and (b) show the models being introduced during gravity field determination whereas Figs 8(c) and (d) illustrate the effect of the models on the residual level.

After this short excursion, we would like to draw the main conclusion of this chapter. We have shown that taking atmospheric model uncertainties into account will not have a significant effect on the current level of KBRR-residuals. This conflicts with our expectations expressed at the end of Section 3.2, where we expressed the hope that an effect of using atmospheric errors in the de-aliasing process on GRACE gravity field determination should be visible. The answer to the question of why there is no effect of atmospheric model errors on the KBRR-residuals becomes obvious in Fig. 10 and leads, after a short summary of the obtained results, to the final conclusions.

4 SUMMARY AND CONCLUSION

This paper has summarized the atmospheric and oceanic de-aliasing process (Section 2.1) as well as an alternative de-aliasing approach (Section 2.3). As the current de-aliasing process does not take into account atmospheric and oceanic model uncertainties, a full error-propagation model, which is capable of including these model errors, was developed (Section 2.2). The impact of atmospheric model uncertainties on the vertically integrated atmospheric pressure was shown in Section 3.1. There it was revealed that uncertainties in the atmospheric model parameters, specific humidity, geopotential and temperature are almost negligible, whereas uncertainties in the surface pressure have the most significant impact on the vertically integrated atmospheric pressure I_n. In Section 3.2, we investigated the effect of errors in the vertically integrated atmospheric pressure on the resulting potential coefficients as well as on the geoid. Figs 4 and 5 illustrated that whether model uncertainties are taken into account or not affects AOD in the sub-mm domain. Concerning the so-called GRACE baseline, it was expected that atmospheric model uncertainties have an effect on GRACE. However as it was shown in Section 3.3, the atmospheric model uncertainties currently do not have a significant effect on GRACE or on KBRR-residuals, respectively. Having a look at Fig. 10, the reason for this becomes obvious: Fig. 10 is identical to Fig. 4, except that it also contains the actual or achieved (as opposed to the expected pre-launch) accuracy of gravity field determination with GRACE (green line). As the differences 'error-free' minus 'full-error' are clearly below the curve 'actual GRACE baseline', it is clear that the impact of the refined AOD model studied here is not visible in gravity field determination. This leads us to the conclusion that—at this point in time—with the current performance of GRACE—atmospheric model uncertainties are not able to improve the de-aliasing process or gravity field determination. It should be kept in mind, however, that model uncertainties will become more important if the actual accuracy of GRACE can be further improved towards the expected baseline by other means. For the time being, this is essentially the final conclusion of this study. Finally, it has to be emphasized that the results are based on data from the operational analysis of the ECMWF. Also, one should take into account that the used error-fields may be too optimistic as they result from the assimilation model (ECMWF 2009) itself and not from individual calibration. In Section 3.1, it was pointed out that the surface pressure error plays the major role. It therefore is essential to determine reliable surface pressure values and to use them as input for the upcoming investigations. Furthermore, the ocean bottom pressure error has been disregarded up to now. Determining reasonable error values for ocean bottom pressure and taking them into account during AOD determination will be subject to further investigations.

ACKNOWLEDGMENTS

This study was carried out in the context of the IDEAL-GRACE project within the SPP1257 priority program 'mass transport and mass distribution in the system Earth', funded by the German Research Foundation (Deutsche Forschungsgemeinschaft).

REFERENCES

Beutler, G., Jäggi, A., Mervart, L. & Meyer, U., 2010. The celestial mechanics approach – application to data of the GRACE mission, *J. Geod.*, in press.

Chen, J., Wilson, C., Tapley, B. & Grand, S., 2007. GRACE detects coseismic and postseismic deformation from the Sumatra-Andaman earthquake, *Geophys. Res. Lett.,* **34,** L13302, doi:10.1029/2007GL030356.

Dach, R., Hugentobler, U., Fridez, P. & Meidl, M., eds, 2007. *Bernese GPS Software,* Astromical Insitute, University Bern, Bern, Switzerland.

Dobslaw, H. & Thomas, M., 2007. Simulation and observation of global ocean mass anomalies, *J. geophys. Res.,* **112**, doi:10.1029/2006JC004035.

ECMWF, 2009. MARS User Guide. Technical Notes, http://www.ecmwf.int/publications/manuals/mars/.

Flechtner, F., 2007. AOD1B product description document, GRACE project documentation, JPL, Pasadena, CA.

Gruber, T., 2001. High resolution gravity field modeling with full variance-covariance matrices, *J. Geod.,* **75**(9-10), 505–514, ISSN 0949-7714.

Han, S., Jekeli, C. & Shum, C., 2004. Time-variable aliasing effects of ocean tides, atmosphere, and continental water mass on monthly mean GRACE gravity field, *J. geophys. Res.,* **109**, doi:10.1029/2003JB002501.

Jäggi, A., Beutler, G., Meyer, U., Prange, L., Dach, R. & Mervart, L., 2010. AIUB-GRACE02S—status of GRACE gravity field recovery using the celestial mechanics approach, in *Geodesy for Planet Earth*, IAG, Springer, in press.

Ponte, R. & Dorandeau, J., 2003. Uncertainties in ECMWF surface pressure fields over the ocean in relation to sea level analysis and modeling, *J. Atmos. Oceanic Technol.,* **20,** 301–307.

Salstein, D., Ponte, R. & Cady-Pereira, K., 2008. Uncertainties in atmospheric surface pressure fields from global analyses, *J. geophys. Res.,* **113**, doi:10.1029/2007JD009531.

Schmidt, T., Wickert, J., Heise, J., Flechtner, F., Fagiolini, E., Schwarz, G., Zenner, L. & Gruber, T., 2008. Comparison of ECMWF analyses with GPS radio occultations from CHAMP, *Ann. Geophys.,* **26**(11), 3225–3234.

Werth, S., Guntner, A., Petrovic, S. & Schmidt, R., 2009. Integration of GRACE mass variations into a global hydrological model, *Earth planet. Sci. Lett.,* **277**(1-2), 166–173.